The Impact of Large-scale Flow Direction on the Formation of a Glacier Boundary Layer

Two Large-eddy Simulation Case Studies

Brigitta Goger, Ivana Stiperski, and the SCHISM* Team

*SCHISM: “Snow Cover Dynamics and High-resolution Modelling” is a joint FWF-DFG project.

The Hintereisferner Glacier (Ötztal Alps, Austria)

Figure 1: Aerial image of the Hintereisferner glacier from September 2019 (Image source)

- World Glacier Monitoring Service reference glacier
- Length: around 6 km
- Spans from the Weißkugel peak (3738 m) to 2460 m
- Long-term mass balance monitoring since 1953 and meteorological observations (Strasser et al., 2018)

Navigation info: External links and references are shown in dark blue.

Motivation and Research Questions

1. Model validation: Is WRF able to simulate the boundary layer evolution over the glacier?

2. Which processes contribute to sensible heat flux heterogeneity and non-stationarity? Are point observations representative for the spatial sensible heat flux structure?

3. Is the glacier boundary layer governed by the synoptic wind direction? What is the role of upstream topography?

Observations

- Permanent stations: South-facing slope (Station Hintereis, StHE) and mountain ridge (Im Hinteren Eis, iHE)
- HEFEX stations (Mott et al., 2020): Spatially distributed eddy-covariance stations on the glacier tongue (measurement campaign in August 2018)

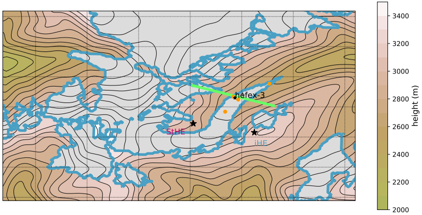

Figure 2: Our region of interest with glacier outlines (light blue) and the observations: Station Hintereis (StHE), Im Hinteren Eis (iHE), and the HEFEX stations. The displayed topography and the glacier outlines are from the innermost model domain (next slide).

Two Case Studies for LES

1. August 7, 2018 (SW day): Synoptic flow from South-West
2. August 17, 2018 (NW day): Synoptic flow from North-West

Large-eddy Simulations with WRF

Domains

- d01: $\Delta x = 6\,\text{km} \rightarrow$ d02: $\Delta x = 1\,\text{km}$
- d03: $\Delta x = 240\,\text{m} \rightarrow$ d04: $\Delta x = 48\,\text{m}$

Figure 3: The mesoscale domain (d02, $\Delta x = 1\,\text{km}$, where the locations of domain 3 ($\Delta x = 240\,\text{m}$, yellow rectangle) and domain 4 ($\Delta x = 48\,\text{m}$, red rectangle) are highlighted.

All model output shown in the following slides is from domain 4.

WRF Model Set-up

(details in appendix [2])

- Nested set-up of four domains
- Two innermost domains in LES mode (d03, d04)
- Start: 03 UTC, runtime: 18 h

d04: LES Set-up

- $\Delta x = 48\,\text{m}$
- Deardorff LES closure
- 15-min online averaging of chosen variables (Umek et al., 2021)
- 86 vertical levels, lowest level at $z = 7\,\text{m}$ a. g.

Timeseries: Glacier Tongue and Surroundings

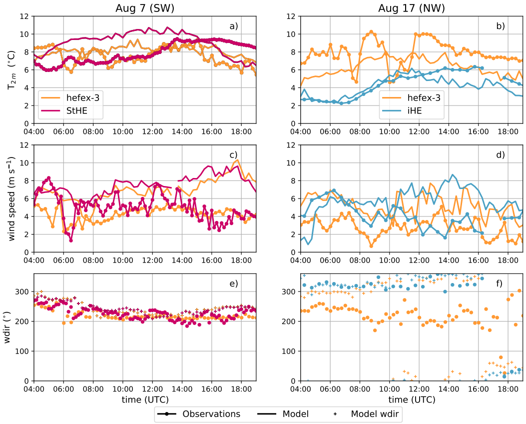

Figure 4: Time series of 2 m temperature (a,b), horizontal wind speed (c,d), and wind direction (e,f) from the SW day (left column) and the NW day (right column). Connected dots indicate observations, while straight lines (or plus signs, respectively) indicate model output. Orange colors show data from the station hefex-3, pink colors indicate StHE, and blue colors indicate iHE.

- Overall, good performance of WRF for general meteorological variables
- Wind speeds are overestimated
- SW day: constant down-glacier flow (hefex-3), also SW influence at StHE.
- NW day: cross-glacier flow with freqent disturbances and NW synoptic flow at the mountain ridge (iHE).

Potential Temperature (Θ) and Wind Field

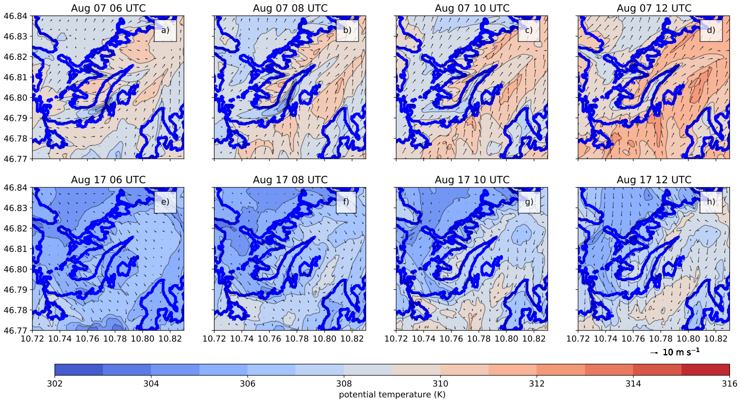

Figure 5: Averaged model output from the lowest model level of potential temperature (colors and black contour lines) and horizontal wind vectors. Blue lines indicate the outlines of the glacier as it is represented in the model domain.

1. SW day (Fig. 5a-d):
   - Spatially inhomogeneous Θ structure
   - Body of potentially colder air over glacier surfaces
2. NW day (Fig. 5e-h):
   - Spatially homogeneous Θ structure
   - Strong cross-glacier flow

Vertical Cross-section across the Glacier

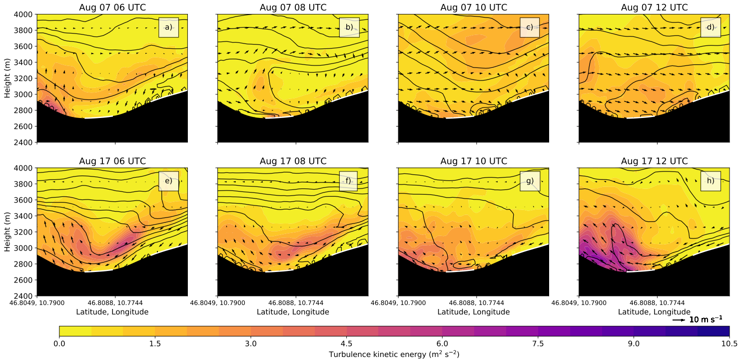

Figure 6: Vertical cross-section along the light-green line in Fig. 2 for the SW day (upper row) and the NW day (lower row). White lines along the topography indicate glaciated areas. Black contour lines show the potential temperature, wind vectors indicate the cross-valley wind speed, and colors indicate resolved turbulence kinetic energy.

1. SW day (Fig. 6a-d):
   - Local glacier ABL (Fig. 6b,c)
   - Locally-generated TKE
2. NW day (Fig. 6e-h):
   - Strong breaking gravity-wave and severe turbulence
   - Elevated TKE maximum
   - Glacier ABL is eroded

Sensible Heat Flux and Wind Field

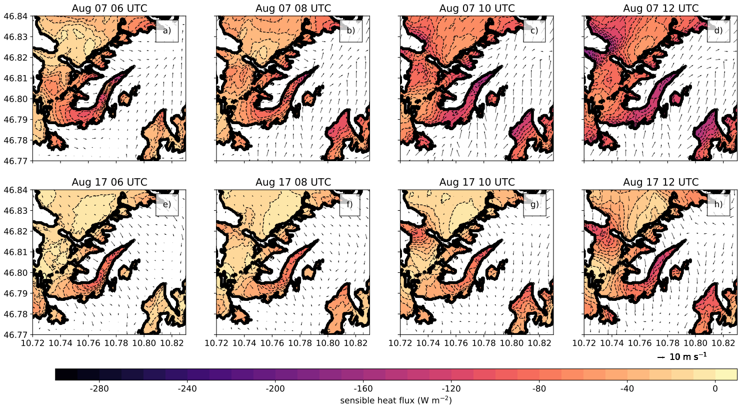

Figure 7: Averaged model output of the surface sensible heat flux (colors and dashed lines) and horizontal wind vectors from the lowest model level over glaciated surfaces. Sensible heat fluxes over ice-free surfaces are not shown.

1. SW day (Fig. 7a-d):
   - SHF structure aligned with wind direction
   - Increased wind speed → high SH
2. NW day (Fig. 7e-h):
   - Generally weaker SHF values than on SW day
   - SHF maximum when gravity wave breaks

Timeseries: Sensible Heat Flux (SHF) and Stationarity

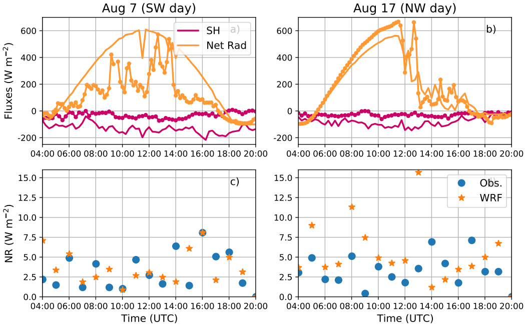

Figure 8: (a,b) Time series of the net radiation from StHE (orange lines) and the surface sensible heat flux of hefex-3 (pink lines) for both case study days, where straight lines show model output and lines with dots show observations. (c,d) NR of the sensible heat flux time series from hefex-3 of one-minute observations (blue points) and one-minute model output (orange stars).

- SHF on both days negative (into the ice) over the glacier (Fig. 8a,b); smaller values on NW day
- Non-stationarity ratio (NR) of SHF (Mahrt, 1998, see also A4):
  - Both timeseries of SHF are non-stationary (NR$>$ 2)
  - SW day: constant non-stationarity
  - NW day: quickly changing non-stationarity $\rightarrow$ strong mesoscale gravity wave influence

Have a look at movies of SHF on the SW day and NW day!

Horizontal Temperature Advection and Streamlines

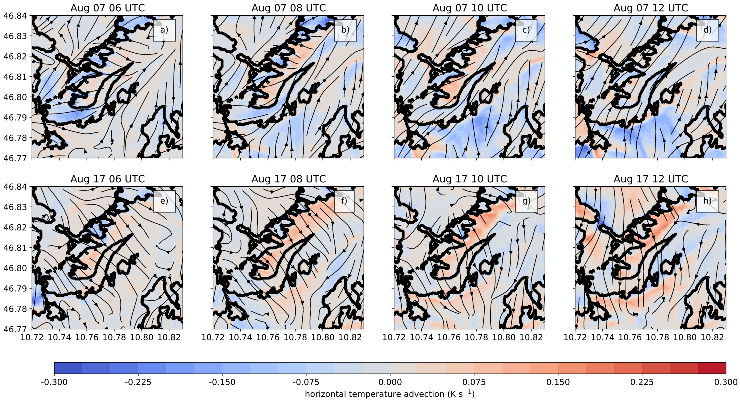

Figure 9: Averaged model output of the averaged horizontal temperature advection (colors) and streamlines derived from the wind field from the lowest model level. The left column shows data from the SW day, while the right column shows data from the NW day, at four different times.

1. SW day (Fig. 7a-d):
   - Cold-air advection over glacier tongue together with down-glacier wind
2. NW day (Fig. 7e-h):
   - Weak warm-air advection dominating the glacier tongue

Scatterplots

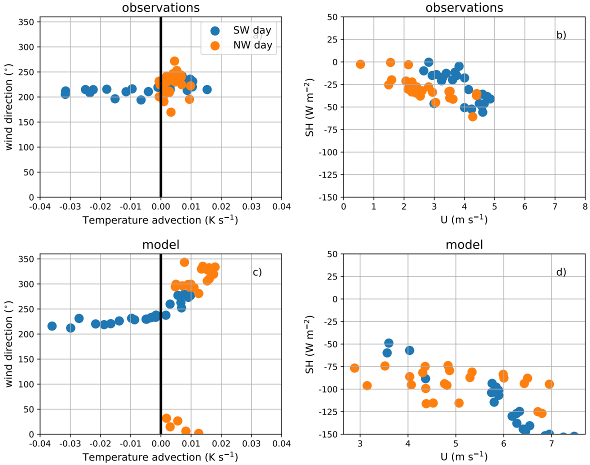

Figure 10: Scatter plots of the SW day and the NW day from observations (upper row) and model output (lower row) from hefex-3 for horizontal temperature advection and wind direction (a,c) and horizontal wind speed and sensible heat flux (b,d).

- Type of temperature advection depends on wind direction (Fig. 9a,c)
- Linear relationship between SHF and horizontal wind speed (Fig. 9b,d)

Summary

Case 1: South-West

- Synoptic flow is aligned with down-glacier wind
- Dominance of local processes allows a glacier boundary layer to form
- Heterogeneous sensible heat flux pattern
- Glacier tongue dominated by cold-air advection (due to down-glacier wind)

Case 2: North-West

- Synoptic flow across the glacier tongue $\rightarrow$ erosion of local glacier boundary layer
- Strong gravity-wave activity with severe turbulence
- Non-stationary sensible heat flux and mesoscale infuence
- Glacier tongue mostly under warm-air advection (cross-glacier flow)

Conclusions and Outlook

1. WRF-LES is able to simulate the general meteorological situation over HEF
2. Synoptic flow direction either supports or erodes the glacier boundary layer
3. Upstream topography governs the formation and strength of gravity waves
4. Sensible heat flux is highly spatially heterogeneous and non-stationary
5. Future work: Winter case studies and the impact of the wind field on snowdrift on the glacier

Want to learn more about the Schism project?
Join A. Voordendag et al.: Uncertainty assessment of a permanent long-range terrestrial laser scanning system at an Alpine glacier

Acknowledgements

This work is part of the project "Measuring and modeling snow-cover dynamics at high resolution for improving distributed mass balance research on mountain glaciers", a joint project fully funded by the Austrian Science Foundation (FWF) and the Deutsche Forschungsgemeinschaft (DFG) under the project number I 3841-N32. Numerical simulations were performed on the Vienna Scientific Cluster (VSC) under project number 71434.

Der Wissenschaftsfonds.

Deutsche Forschungsgemeinschaft

References

Mahrt, L., 1998: Flux Sampling Errors for Aircraft and Towers. *J. Atmos. Ocean. Technol.*, **15 (2)**, 416 – 429, `doi:10.1175/1520-0426(1998)015<0416:FSEFAA>2.0.CO;2`.

Mott, R., I. Stiperski, L. Nicholson, and J. Mertes, 2020: Spatio-temporal flow variations driving heat exchange processes at a mountain glacier. *The Cryosphere*, **14**, 4699–4718, `doi:10.5194/tc-2020-78`.

Strasser, U., et al., 2018: The Rofental: a high Alpine research basin (1890–3770 m a.s.l.) in the Ötztal Alps (Austria) with over 150 years of hydrometeorological and glaciological observations. *Earth Syst. Sci. Data*, **10 (1)**, 151–171, `doi:10.5194/essd-10-151-2018`.

Umek, L., A. Gohm, M. Haid, H. C. Ward, and M. W. Rotach, 2021: Large eddy simulation of foehn-cold pool interactions in the Inn Valley during PIANO IOP2. *Q. J. R. Meteor. Soc.*, `doi:https://doi.org/10.1002/qj.3954`.

Appendix

Model Set-up I

- Model runtime: 18 hrs, 03 UTC – 21 UTC (restart around 14 UTC)
- ERA5 data $\rightarrow$ d01 $\rightarrow$ d02 $\rightarrow$ (ndown) $\rightarrow$ d03 (LES) $\rightarrow$ d04 (LES)

Static data

- STRM Topography, 4 smoothing cycles applied (1-2-1 smooting)
- Soil: Harmonized world soil database
- Land-use:
  ESA-CCI data (d01,d02)
  CORINE data (d03,d04)
- Land-Use for LES domains modified with glacier shapefiles from the Randolph Glacier Inventory (RGI) and a Hintereisferner shapefile from 2018 (thanks to Rainer Prinz)

Model Set-up II

Parameterizations (WRF physics references)

- d01, d02 (Mesoscale simulation): MYNN PBL Parameterization
- d03, d04 (LES): no PBL scheme, Deardorff LES closure
- Surface layer: MM5 scheme
- Land surface: NOAH-MP
- Microphysics: Thompson scheme
- Radiation: CAM Shortwave and Longwave Schemes + topographic shading

Non-stationarity ratio I

After Mahrt (1998): For the one-minute timeseries of both model and observations, we divide the one-minute timeseries in 15-minute sub-intervals (j=72) consiting of i=15 sub-records, and calculate the within-record variability:

$$\sigma_{k,wi}(i) = \sqrt{\frac{1}{J-1}\sum_{j=1}^{J}[F_k(i,j) - F_k(i)]^2}, \quad (1)$$

With the average of the sensible heat fux for each pass being

$$F_k(i) = \frac{1}{J}\sum_{j=1}^{J} F_k(i,j), \quad (2)$$

Non-stationarity ratio II

after the averaging of the standard deviation.

$$\sigma_{k,wi}(i) = \frac{1}{I}\sum_{i=1}^{I}\sigma_k(i), \tag{3}$$

The standard error of the passed-averaged flux results:

$$RE_k = \frac{\sigma_{k,wi}}{\sqrt{J}}. \tag{4}$$

Now the standard deviation for the pass-averaged flux can be obtained,

$$\sigma_{k,btw}(i) = \sqrt{\frac{1}{I-1}\sum_{i=1}^{J}[F_k(i) - F_k]^2}, \tag{5}$$

Non-stationarity ratio III

and the non-stationarity ratio results as:

$$NR = \frac{\sigma_{k,btw}}{RE_k} \tag{6}$$

1. $NR \approx 1$: stationarity can be assumed
2. $NR > 2$: non-stationarity can be assumed